Chemical Physics 375 (2010) 410–415

Contents lists available at ScienceDirect

Chemical Physics

journal homepage: www.elsevier.com/locate/chemphys

Stochastic resonance in a surface dipole

E. Heinsalu [a,b,*], M. Patriarca [a,b], F. Marchesoni [c]

[a] IFISC, Instituto de Física Interdisciplinar y Sistemas Complejos (CSIC-UIB), E-07122 Palma de Mallorca, Spain
[b] National Institute of Chemical Physics and Biophysics, Rävala 10, 15042 Tallinn, Estonia
[c] Dipartimento di Fisica, Università di Camerino, I-62032 Camerino, Italy

ARTICLE INFO

Article history:
Received 18 January 2010
In final form 13 March 2010
Available online 27 March 2010

Keywords:
Stochastic resonance
Surface diffusion
Electric dipole

ABSTRACT

The dynamics of a neutral dipole diffusing on a one-dimensional symmetric periodic substrate is numerically investigated in the presence of an ac electric field. It is observed that the amplitude of the forced oscillations of the dipole can be enhanced by tuning the noise strength, i.e., the substrate temperature. Such a manifestation of stochastic resonance turns out to be extremely sensitive to the mechanical properties of the dipole. This phenomenon has immediate applications in surface physics and nanodevice technology.

1. Introduction

In this paper we study the diffusion of neutral short chain segments moving on a one-dimensional (1D) periodic symmetric substrates. We model the chain segments as overdamped neutral dipoles, or dimers, made up of two bound equal pointlike masses, or monomers, carrying opposite charges and suspended in a viscous medium. Elastic dimers of this kind can be used to represent, for instance, tiny fragments of longer and more complex molecular chains, as is often the case in DNA electrophoresis [1], or neutral molecular segments stretched between two charged synthetic beads [2].

Contrary to the case of a dimer in which the external field acts in the same way on both monomers [3,4], in the case of a neutral dipole an external electric field pulls the monomers to opposite directions, as sketched in Fig. 1. The field, no matter whether dc or ac, cannot induce a net dipole current, since the total force applied to the neutral dipole center of mass is zero, and the underlying substrate is assumed to be symmetric under space inversion. A significant exception is represented by devices where the diffusion is constrained by an asymmetric geometry [5]. As a consequence, the motion of the center of mass on a symmetric substrate is purely diffusive [6,7]. However, the internal degree of freedom of a dipole, when constrained to 1D and subjected to an oscillating field of force, exhibits interesting properties, which result from the interplay of monomer–substrate and monomer–monomer interactions. Such properties can be relevant to a variety of physical and biological systems, where the particle dynamics is naturally overdamped and constrained to (quasi) 1D substrates [6]. Related topics of ongoing research include colloids [8] or cold atoms [9] in optical traps, superconducting vortices in lithographed tracks [10], ion-channels [11], cell membranes [12], artificial and natural nanopores [13], etc. Moreover, one is interested in the dimer dynamics in the force direction (directed dimer) even when dealing with dimers periodically driven on a two-dimensional (2D) substrate, as long as the transverse diffusion is not significantly affected by the drive (for a review see Ref. [6]).

The main result of this paper is that, at variance with the case of a single monomer in a periodic potential [14], a directed neutral dipole exhibits Stochastic Resonance (SR) [15,16]. The simplest dynamical system displaying SR is a Brownian particle diffusing in a bistable potential under the simultaneous action of a time oscillating tilt and a fluctuating force (noise). In the system consisting of a neutral dipole on a periodic potential, bistability occurs as a purely geometric effect, as in 1D the dipole heads can exchange coordinates by overcoming a finite repulsive energy barrier, which results from the combined action of the substrate potential and dipole binding potential. Moreover, the role of the Brownian monomer coordinate is played here by the relative coordinate of the dipole constituents, so that the amplitude of the forced oscillations of a directed dipole sitting on a periodic substrate can be optimized by tuning the noise strength (i.e., the temperature in the case of thermal noise). Furthermore, according to our numerical simulations, such an effect is extremely sensitive to the details of the dimer binding potential. In conclusion, the SR mechanism we report in this paper is highly selective with respect to the length and elasticity of the dipole, so that it can have important technological applications.

* Corresponding author at: IFISC, Instituto de Física Interdisciplinar y Sistemas Complejos (CSIC-UIB), E-07122 Palma de Mallorca, Spain.
E-mail address: els@ifisc.uib-csic.es (E. Heinsalu).

0301-0104/$ - see front matter © 2010 Elsevier B.V. All rights reserved.
doi:10.1016/j.chemphys.2010.03.013

Fig. 1. Scheme of the system under study: A neutral dipole composed of two interacting oppositely charged monomers moving on a periodic substrate under the action of an ac electric field $E(t)$.

This paper is organized as follows. In Section 2 we introduce the model (Section 2.1), define the units, characterize the diffusion of a neutral dipole on a sinusoidal substrate in both fully 2D (Section 2.2) and reduced 1D formalism (Section 2.3), and outline the numerical algorithms employed in our investigation (Section 2.4). A quantitative analysis of the dipole SR phenomenon is presented in Section 3, with particular emphasis on the role of the binding potential. Remarkably, a SR peak was detected for hard binding potentials, like the quartic potentials of Sections 3.2 and 3.3, but not for the quadratic potentials of Section 3.1. Potential applications of the SR mechanism to neutral dipoles and/or short molecular chains on a surface are discussed in Section 4.

2. Model

Earlier reports have already addressed some of the properties of the dimer model we introduce in this section. Most notable examples are the Brownian motion of rigid dimers with constant length in either 2D symmetric [17] or 1D asymmetric potentials [18,19], and the effects of length oscillations on the mobility and diffusion of a damped dimer [20,21,4,22,3]. However, no particular attention was paid to the dimer internal dynamics, which is the main subject of the present investigation.

2.1. Langevin formulation

We study a Brownian dipole composed of two monomers with equal masses, m, and opposite charges, $q_1 = -q_2 = -q$ and $q > 0$. Monomers move in a 1D periodic substrate potential, $U_0(x) = U_0(x + L)$, subject to an external ac electric field, $E(t)$. This model, schematically depicted in Fig. 1, is described by two coupled Langevin equations,

$$\begin{aligned} m\ddot{x}_1 &= -\frac{\partial U(x_1,x_2,t)}{\partial x_1} - \eta\dot{x}_1 + \xi_1(t), \\ m\ddot{x}_2 &= -\frac{\partial U(x_1,x_2,t)}{\partial x_2} - \eta\dot{x}_2 + \xi_2(t). \end{aligned} \tag{1}$$

Here η is the viscous friction coefficient, while $\xi_i(t)$, with $i = 1, 2$, represent the thermal fluctuations exerted by the substrate in equilibrium at a fixed temperature T; $\xi_i(t)$ are modeled as independent Gaussian white noises with zero mean and auto-correlation functions

$$\langle \xi_i(t)\xi_j(t')\rangle = 2\eta k_B T\delta_{ij}\delta(t-t'), \quad i,j = 1,2. \tag{2}$$

The total potential, $U(x_1, x_2, t)$, takes into account the monomer–substrate and monomer–monomer interactions, as well as the external electric potential, that is

$$U(x_1,x_2,t) = U_0(x_1) + U_0(x_2) + U_{\rm int}(x_2 - x_1) - qE(t)(x_2 - x_1). \tag{3}$$

For the periodic substrate potential acting upon the ith monomer we assume a simple sinusoidal function,

$$U_0(x_i) = -A_0\cos(kx_i), \tag{4}$$

with amplitude A_0, length constant $L = 2\pi/k$, and a minimum at the origin, $U_0(x_i = 0) = -A_0$. As for the interaction potential, we will consider two standard cases: the quadratic interaction (quadratic dimer),

$$U_{\rm int}(x_2 - x_1) = \frac{K_2}{2}(x_2 - x_1 - a_0)^2 \tag{5}$$

and the quartic interaction (quartic dimer),

$$U_{\rm int}(x_2 - x_1) = \frac{K_4}{4}(x_2 - x_1 - a_0)^4, \tag{6}$$

where $a_0 \geqslant 0$ is the equilibrium monomer distance, or dimer length, and K_2, K_4 are tunable interaction, or coupling, constants. The time-periodic electric field has a sinusoidal waveform,

$$E(t) = E_0\sin(2\pi\nu t), \tag{7}$$

with amplitude E_0 and frequency ν. In the following we refer to $F_0 = qE_0$ as to the amplitude of the force, $F(t) = \pm qE(t)$, applied to the monomers.

2.2. Dipole dynamics as a 2D problem

The 1D motion of the Brownian dipole can be mapped into the 2D motion of a single Brownian particle in the x_1–x_2 plane. For convenience, we also introduce the x–y plane defined by the center of mass coordinate, x, and the instantaneous half-length, y, of the dimer, i.e.,

$$x = (x_1 + x_2)/2, \quad y = (x_2 - x_1)/2. \tag{8}$$

The coordinate change $(x_1, x_2) \to (x, y)$ is equivalent to rotating the x_1–x_2 frame by an angle $\pi/4$ and rescaling the coordinate units by a factor $1/\sqrt{2}$. On inserting the potential functions (3) and (4) into Eq. (1), the Langevin equations in the new coordinates read

$$\begin{aligned} m\ddot{x} &= -A_0k\sin(kx)\cos(ky) - \eta\dot{x} + R_x(t), \\ m\ddot{y} &= -A_0k\cos(kx)\sin(ky) - U'_{\rm int}(2y) + qE(t) - \eta\dot{y} + R_y(t), \end{aligned} \tag{9}$$

where $U'_{\rm int}(y) = dU_{\rm int}(y)/dy$. The two random forces,

$$R_x(t) = [\xi_1(t) + \xi_2(t)]/2, \quad R_y(t) = [\xi_2(t) - \xi_1(t)]/2, \tag{10}$$

are uncorrelated and characterized by the same effective temperature $T/4$, namely,

$$\begin{aligned} &\langle R_x(t)\rangle = \langle R_y(t)\rangle = 0, \quad \langle R_x(t)R_y(t')\rangle = 0, \\ &\langle R_x(t)R_x(t')\rangle = \langle R_y(t)R_y(t')\rangle = (\eta T/2)\delta(t-t'). \end{aligned} \tag{11}$$

The 2D potential corresponding to the conservative forces in the Langevin Eq. (9),

$$U(x,y,t) = -A_0\cos(kx)\cos(ky) + U_{\rm int}(2y)/2 - qE(t)y \tag{12}$$

is plotted in Fig. 2(b) for a quartic dimer with zero equilibrium length and in the absence of an external field. Note that the center of mass coordinate x enters $U(x, y, t)$ only through the substrate term. As a consequence, the x dependence of the minima of the relevant potential surface, panel (a) of Fig. 2, is determined by the substrate potential U_0, alone. From the extremum conditions for $U(x, y, t)$, at a given time t,

$$\frac{\partial U}{\partial x} = A_0k\sin(kx)\cos(ky) = 0, \tag{13}$$

$$\frac{\partial U}{\partial y} = A_0k\cos(kx)\sin(ky) + U'_{\rm int}(2y) - qE(t) = 0, \tag{14}$$

it follows that the extremes of this potential have coordinates $x_n = n(L/2)$ with integer n, corresponding to a maximum for odd n, and to a minimum for even n (see panel (b) of Fig. 2). On inserting the solution $x_n = n(L/2)$ of Eq. (13) into Eq. (14), one obtains the following equation for y_n,

$$\pm A_0k\sin(y_n) + U'_{\rm int}(2y_n) - qE(t) = 0. \tag{15}$$

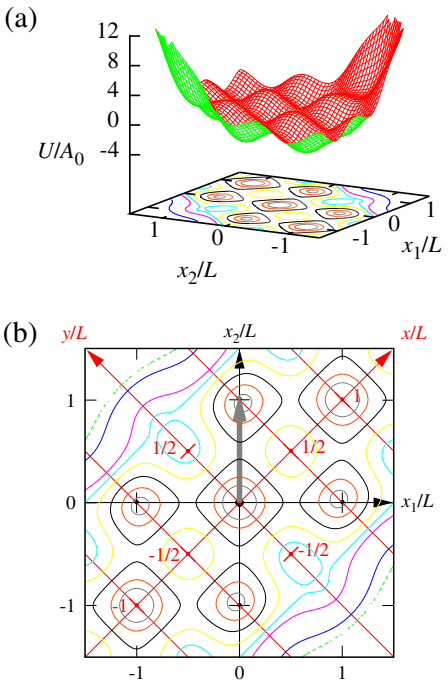

Fig. 2. (a) Surface and contour plot of the potential U given by Eq. (3) with Eqs. (4) and (6) in the x_1–x_2 coordinate frame, for zero drive, $E = 0$, zero equilibrium length, $a_0 = 0$, and rescaled coupling constant $K_4 = 10^{-3}$. (b) Countour plot of the same potential as in panel (a): comparison in the x–y and x_1–x_2 coordinate frames. The stable regions are located by darker closed contour lines. The thick arrow represents an example of most probable transition, i.e., from the origin $(x,y) = (0,0)$ to the nearest neighbor minimum $(L/2, L/2)$.

The solutions for y_n are very sensitive to the interaction potential, $U_{\rm int}$, and the external force, F_0. In the absence of the interaction potential, $U_{\rm int} = 0$, and the electric field, $E = 0$, the potential (3) is an egg-carton potential with the minima located at $(x,y) = (nL/2, mL/2)$, with integer n, m. Introducing the interaction (5) or (6) produces a distortion of the periodic egg-carton potential in the y-direction, see Fig. 2. Whereas, the coordinates of the minima lying on the x-axis remain unchanged, the positions of the other minima are shifted or the minima disappear (see Fig. 2(b)).

One may now ask what are the most probable transitions of the system in the potential energy landscape of Fig. 2. Let us consider the x–y frame and assume that the starting configuration coincides with the equilibrium point at $(x,y) = (0,0)$. By inspecting the contour lines in Fig. 2(b), one concludes that the most favored transitions are those from $(0,0)$ toward one of the four nearest neighbor minima $(\pm L/2, \pm L/2)$. Indeed, such transitions require overcoming lower and narrower potential barriers than, for instance, the next-to-nearest neighbor transitions, $(0,0) \to (\pm L, 0)$. The transitions $(0,0) \to (\pm L/2, \pm L/2)$ correspond to the situation when one monomer sits at the origin (either $x_1 = 0$ or $x_2 = 0$), while the other one jumps into a neighbor valley ($x_2 \approx \pm L$ or $x_1 \approx \pm L$). If also the external ac electric field is applied, the potential surface undergoes a periodic tilting around the x-axis (see Eq. (12)), thus favoring alternately transitions toward minima with $y = L/2$ and $y = -L/2$.

The $(0,0) \to (\pm L, 0)$ transitions describe a monomer coherently jumping from the origin into one of the two adjacent valleys; they are energetically unfavorable and, moreover, cannot be assisted by the external field, which does not couple to the x coordinate. In the x_1–x_2 plane the system will preferably move through a series of vertical and horizontal steps. Diagonal steps representing next-to-neighbor transitions will be highly suppressed. The sample of stochastic trajectory shown in Fig. 3 clearly illustrates this dimer diffusion mechanism (see also Refs. [23,24]).

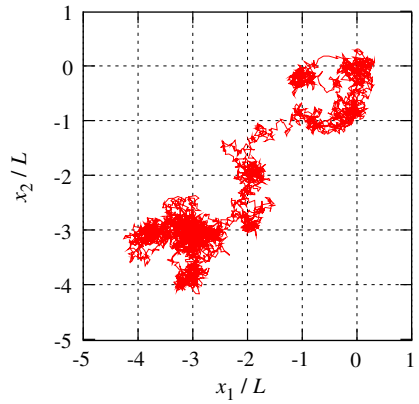

Fig. 3. Sample of stochastic trajectory with initial conditions $(x_1, x_2) = (0,0)$ from numerical integration of Eq. (1) at a resonant temperature $T = 0.9$. The quartic monomer–monomer interaction (6) has been used with $K_4 = 0.008$. Other simulation parameters are: $a_0 = 0$, $F_0 = 0.5$, and $v = 0.02$.

2.3. Effective 1D dynamics

The previous section suggest an approximate 1D picture of the system dynamics. On assuming, without loss of generality, that the dimer motion sets out at the equilibrium point $(0,0)$, the first most probable transitions are oriented toward one of the four nearest neighbor minima marked in Fig. 2(b).

On considering, for example, the transition $(x,y) = (0,0) \to (L/2, L/2)$ [thick arrow in Fig. 2(b)] one can introduce the coordinate s along the transition path, which coincides with x_2 since $x_1 = 0$. Therefore, $x = y = s/2$ (see Eq. (8)) and in the zero temperature limit Eq. (12) yields the approximate effective potential $U_s(s,t)$,

$$U_s(s,t) = 2U(s/2, s/2, t) = -2A_0[\cos(ks/2)]^2 + U_{\rm int}(s) - qE(t)s. \quad (16)$$

This potential motivated us to search for SR evidence. The shape of $U_s(s,t)$ results from the interplay between (i) the periodic substrate potential, (ii) the monomer–monomer interaction potential, and (iii) the external field. For too large F_0 or K_q, with $q = 2, 4$, the potential is monostable, whereas in the opposite limit it becomes multistable with many minima. The dimer length a_0 also plays a role as discussed in Section 3.3. More interesting is the case plotted in Fig. 4, for $a_0 = 0$ and three representative values of the tilt $F(t)$. For $F(t) = 0$ ($t = 0$ and $t = \tau/2$) $U_s(s,t)$ is symmetric with the central

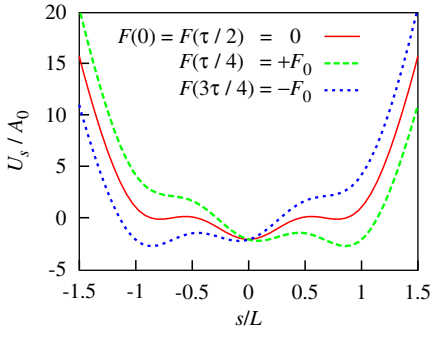

Fig. 4. Effective 1D potential $U_s(s,t)$, Eq. (16), at times $t = 0$ (symmetric), $\tau/4$ ($F = F_0$, maximum tilt to the right), $\tau/2$ (symmetric), and $3\tau/4$ ($F = -F_0$, maximum tilt to the left). The quartic monomer–monomer interaction (6) has been used with $K_4 = 0.008$. Other interaction parameters are: $F_0 = 0.5$ and $a_0 = 0$. In the interval [0,1] U_s approximates the total potential acting on the dimer heads during the transition $(0,0) \to (L/2, L/2)$, see Fig. 2(b).

minimum at $s = 0$ being the deepest; here $\tau = 1/\nu$ is the period of the electric field $E(t)$, Eq. (7). However, due to the sinusoidal character of the electric field $E(t)$, the system spends most time in one of the maximally tilted configurations with $F(t = \tau/4) \approx F_0$ or $F(t = 3\tau/4) \approx -F_0$. In such configurations, either the left or the right minimum disappear and the potential turns bistable. Moreover, the system switches between maximally tilted configurations relatively fast, so that SR manifestations are more likely in those configurations.

Taking into account thermal fluctuations one can arrive at a similar approximation by focusing on the internal degree of freedom, y, and analyzing the effective potential $\langle U(y,t)\rangle$, obtained by averaging the total potential $U(x,y,t)$ with respect to the center of mass coordinate, x (the average can be limited to one unit cell L),

$$\begin{aligned}\langle U(y,t)\rangle &\equiv \langle U(x,y,t)\rangle_x \\ &= -A_0\langle\cos(kx)\rangle_x \cos(ky) + U_{\rm int}(2y)/2 - qE(t)y. \end{aligned} \tag{17}$$

Simple algebraic manipulations yield $\langle\cos(kx)\rangle_x = I_1(\alpha)/I_0(\alpha)$ where $\alpha = (A_0/k_BT)\cos(ky)$ and $I_n(x)$ is the modified Bessel function of order n. The average has been taken at $t = 0$, when $E(t)$ coincides with its average value $E = 0$. For $\alpha \ll 1$, $I_1(\alpha)/I_0(\alpha) \approx \alpha/2 = (A_0/2k_BT)\cos(ky)$ and the effective potential can be approximated to

$$\langle U(y,t)\rangle \approx -\left(A_0^2/2k_BT\right)\cos^2(ky) + U_{\rm int}(2y)/2 - qE(t)y. \tag{18}$$

2.4. Numerical simulations

For numerical simulations, the Langevin Eq. (1) have been first reformulated in terms of the intrinsic space, energy, and time units,

$$\lambda_0 = 1/k, \quad \epsilon_0 = A_0, \quad \tau_0 = \sqrt{\lambda_0^2 m/\epsilon_0}, \tag{19}$$

respectively. The definition of τ_0 ensures that the rescaled monomer masses are equal to one. The units (19) were used to define the dimensionless quantities

$$\begin{aligned}&\tilde t = \frac{t}{\tau_0}, \quad \tilde x_i = \frac{x_i}{\lambda_0}, \quad \tilde x = \frac{x}{\lambda_0}, \quad \tilde y = \frac{y}{\lambda_0}, \quad \tilde a_0 = \frac{a_0}{\lambda_0},\\ &\tilde\nu = \nu\tau_0, \quad \tilde F_0 = \frac{\lambda_0 qE_0}{\epsilon_0}, \quad \tilde F(t) = \tilde F_0\sin(2\pi\tilde\nu\tilde t),\\ &\tilde\xi_i = \frac{\lambda}{\epsilon_0}\xi_i, \quad \widetilde R_{x,y} = \frac{\lambda}{\epsilon_0}R_{x,y}, \quad \widetilde T = \frac{k_BT}{\epsilon_0}, \quad \tilde\gamma = \frac{\eta\tau_0}{m},\\ &\widetilde U'_{\rm int}(\tilde y) = \frac{\lambda}{\epsilon_0}U'_{\rm int}(\lambda\tilde y) = \frac{\widetilde K_q}{q}(\tilde y - \tilde a_0)^q \quad (q = 2,4). \end{aligned} \tag{20}$$

The coupling constants of $\widetilde U_{\rm int}$ were rescaled as $\widetilde{K_2} = \lambda_0^2K_2/\epsilon_0$, for the quadratic interaction ($q = 2$), and $\widetilde{K_4} = \lambda_0^4K_4/\epsilon_0$, for the quartic interaction ($q = 4$).

For simplicity, in the following sections we drop the tildes altogether. The rescaled Langevin Eq. (1) thus read

$$\begin{aligned}\ddot x_1 &= -\gamma\dot x_1 - \sin x_1 + F(t) + U'_{\rm int}(x_2 - x_1) + \xi_1(t),\\ \ddot x_2 &= -\gamma\dot x_2 - \sin x_2 - F(t) - U'_{\rm int}(x_2 - x_1) + \xi_2(t), \end{aligned} \tag{21}$$

where $\langle\xi_i(t)\rangle = 0$ and $\langle\xi_i(t)\xi_j(t')\rangle = 2\gamma T\delta_{ij}\delta(t - t')$.

The damped dimensionless Langevin Eq. (21) have been integrated numerically through a standard Milstein algorithm [25]. Individual stochastic trajectories were simulated for different time lengths and time steps, so as to ensure appropriate numerical accuracy. Average quantities have been obtained as ensemble averages over 10^4 trajectories with initial conditions (0,0); transients effects have been estimated and subtracted.

3. Results

In this section we present our numerical results for two classes of dipoles, respectively with quadratic, Eq. (5), and quartic binding potential, Eq. (6). We discuss in particular the time dependence of the stochastic averages of the internal coordinate. In the presence of an ac electric field, $\langle y(t)\rangle$ was fitted by the simple sinusoidal function

$$\langle y(t)\rangle = Y_0\cos(2\pi\nu t + \phi), \tag{22}$$

with appropriate T dependent amplitude, Y_0, and phase, ϕ. The observable Y_0 coincides (in linear response theory approximation) with the amplitude of the first Fourier component of $\langle y(t)\rangle$ and, therefore, is best suitable to provide a direct signature of the SR phenomenon [15].

3.1. Quadratic interaction

In the presence of quadratic monomer interaction, Eq. (5), we found no SR evidence throughout the parameters space we explored. A selection of curves of Y_0 versus T are displayed in Fig. 5 for a zero-length dipole, $a_0 = 0$, for different F_0, ν, and K_2. The curves of $Y_0(T)$ increase monotonically with increasing T and eventually reach a plateau at high temperatures. This was the case even when the parameters in Eq. (5) were chosen so as to approximate as closely as possible the shape of the wells and barrier(s) of the quartic potential in Eq. (6), for which SR was observed.

The absence of SR in a quadratic dimer is not accidental, but reflects a general property of this binding potential. It has been shown in Ref. [26] that a necessary condition for SR to occur in a bistable potential, $U(x)$, is that $U(x)$ grows asymptotically faster than quadratic, i.e., $U(x) \propto |x|^q$, with $q > 2$, at large distances from its minima, $|x| \to \infty$. It is only under this condition that Y_0 gets suppressed both in the limit of large and small T, thus implying the existence of an optimal SR temperature, for which Y_0 goes through a maximum.

Harmonic potentials, with $q = 2$, are a special class of symmetric bistable potentials. They separate hard potentials with a $q > 2$, for which SR has been reported in the earlier literature [15], from soft potentials with $q < 2$, where SR is suppressed by infinite return times and slow thermalization. For $q = 2$, an horizontal Y_0 asymptote was observed at large temperatures [26], as also shown in Fig. 5.

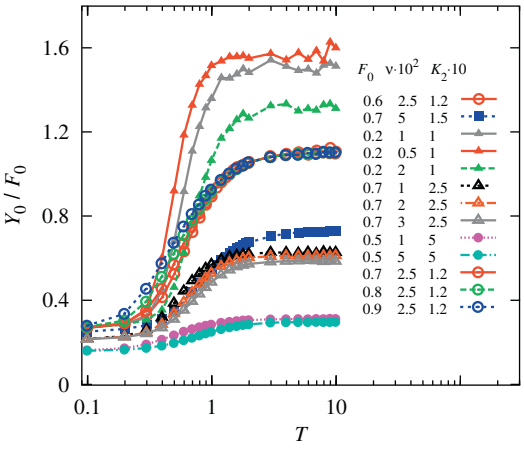

Fig. 5. Zero-length quadratic dimers: Y_0 vs. T for different parameter sets, as reported in the legends. The amplitude Y_0 was obtained by best fitting the linear response theory law (22) to our simulation data for $\langle y(t)\rangle$.

No evidence of SR was detected either in the case of quadratic dimers of finite length (no illustration shown), as $a_0 > 0$ does not change the confining properties of the potential.

3.2. Quartic interaction with $a_0 = 0$

We consider now two monomers interacting through the quartic potential of Eq. (6). For the reasons discussed in the previous section, we expect quartic dimers to exhibit SR [26].

A sample of a quartic dipole stochastic trajectory in the x_1–x_2 plane is displayed in Fig. 3. While the center of mass of the dipole diffuses along the line $y = 0$, or $x_1 = x_2$, due to the hard interaction potential, the relative monomer distance remains tightly bounded, namely, the diffusion process is confined to the neighborhood of the x-axis. For the parameter values used in our simulations, see Fig. 2(b), only the minima located close to $y = 0, \pm L$ are preserved, while all the others disappear. Actually, the system spends most time in the minima sitting on the axis $y = 0$; these are the lowest minima and exist for any tilt $F(t)$. In fact, the system jumps among them in order to move from the leftmost to the rightmost minimum of the effective 1D potential, $U_s(s,t)$ in Fig. 4, and vice versa.

Our fitted amplitudes, Y_0 versus T, are reported in Fig. 6 for different frequencies of the external force. The resonant peak is enhanced at small frequencies. In Fig. 7 different values of the force amplitude are considered. For large F_0 the SR peak is replaced by a low temperature plateau. We have checked that such plateau, at around $F_0 = 1.5$ in the top figure panel, is related to the disappearance of the barrier separating the central from the lateral minima of the effective potential $U_s(s,t)$. Finally, in Fig. 8 we varied K_4 in order to modulate the multistable profile of the effective potential $U_s(s,t)$. As to be expected, for large coupling constants, the lateral minima of the potential vanish (see inset in Fig. 8) and so does the SR peak of $Y_0(T)$.

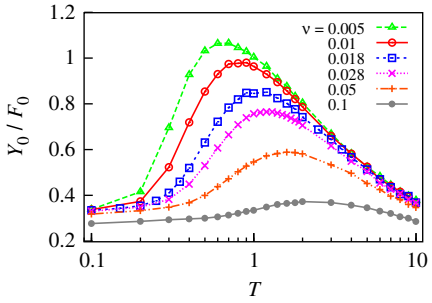

Fig. 6. Zero-length quartic dimers: Y_0 vs. T for different frequencies of the external force (in the legend). Other simulation parameters are: $F_0 = 0.5$ and $K_4 = 0.008$.

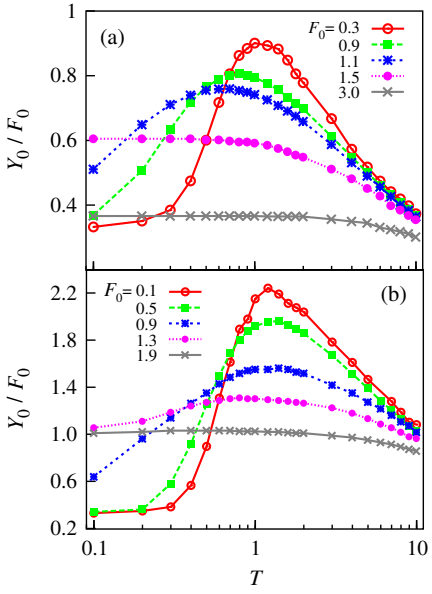

Fig. 7. Zero-length quartic dimers: Y_0 vs. T for different values of F_0 (in the legends). Other simulation parameters are: (a) $\nu = 0.018$, $K_4 = 0.08$ and (b) $\nu = 0.01$, $K_4 = 0.001$.

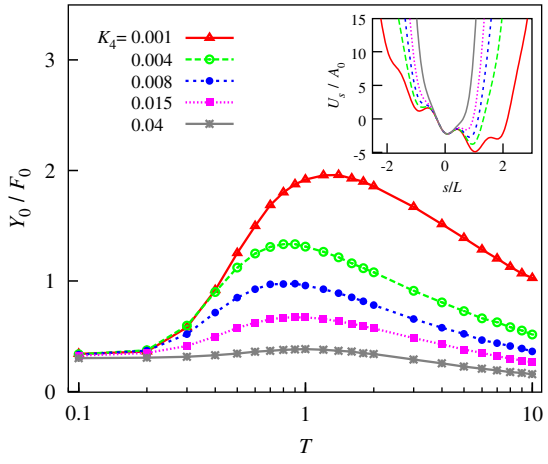

Fig. 8. Zero-length quartic dimers: Y_0 vs. T for different values of K_4 (in the legend). Other simulation parameters are: $F_0 = 0.5$ and $\nu = 0.01$. Inset: Maximum right tilt configurations, $U_s(s)$, of the effective potential $U_s(s,t)$, Eq. (16).

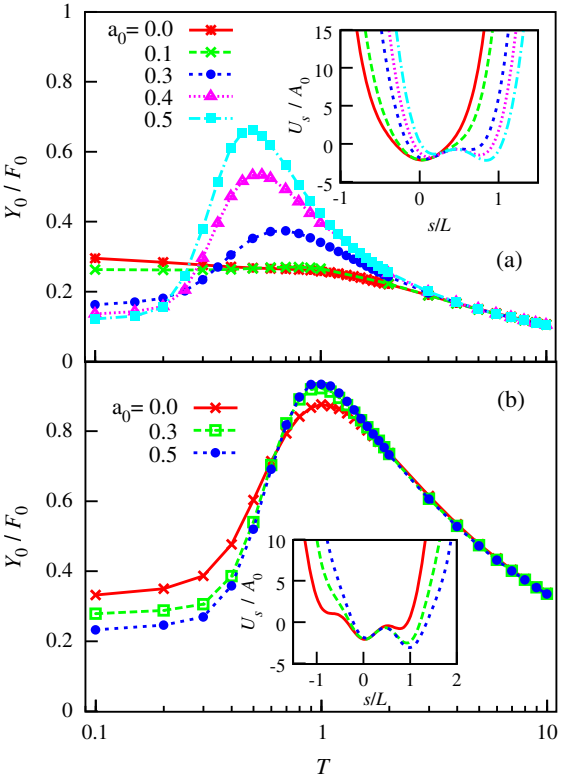

Fig. 9. Amplitude Y_0 vs. T for a quartic dipole with different values of a_0 (in the legends). Insets: Maximum right tilt configuration, $U_s(s)$, of the effective potential in Eq. (16) for the given values of a_0. Other simulation parameters are: (a) $\nu = 0.005$, $K_4 = 0.1$ and (b) $\nu = 0.01$, $K_4 = 0.01$; $F_0 = 0.2$.

3.3. Quartic interaction with $a_0 > 0$

In order to appreciate the role of the dimer length, we have simulated dipoles with quartic monomer–monomer interaction and nonzero length, $a_0 \neq 0$. Note that the results obtained for a certain a_0 are equivalent to those for an equilibrium length $a_0 + nL$, with an integer n. Furthermore, the dynamics of the system is the same for a given $a_0 \in (0, L)$ and for the complementary value $L - a_0$. Therefore, it is sufficient to consider equilibrium distances in the range $(0, L/2)$ only (see Refs. [3,4]).

The diffusion of finite length dipoles strongly depends on the ratio a_0/L, and so does the appearance of SR. The response of the system for different interaction parameters and equilibrium lengths is illustrated in Fig. 9. Note, first, that in the top panel, no SR peak is visible for large K_4 and zero a_0, since the corresponding effective potential, $U_s(s,t)$, is monostable. However, setting a finite dimer length, $a_0 > 0$, causes an asymmetric distortion of $U_s(s,t)$, which may restore a double-well potential structure and, therefore, the conditions for SR to take place. This can be seen by comparing the 1D potentials (16) for the parameters used in the top panel for the limiting cases of zero and maximum length, $a_0 = L/2$ (see inset in Fig. 9(a)). On the contrary, for the small interaction constants used in the bottom panel, a_0 seems to have no remarkable influence on the system response: the potential always has more than one minimum (see inset in Fig. 9(b)), and SR was detected for all a_0 considered.

4. Conclusions

In this paper we have studied the occurrence of SR for neutral dipoles confined on a periodic substrate. The combination of dipole binding and substrate generates the bistable (or multistable) effective potential necessary for the manifestation of SR.

Such a phenomenon can be interpreted as a thermally induced resonance, where the amplitude of the forced oscillations of a directed dipole attains a maximum at an optimal substrate temperature. Let us consider, for instance, an assembly of two species of adatoms carrying opposite charges and arranged so as to form neutral bound pairs, with finite dipole moment, on a crystal surface. Suppose, next, that the surface is irradiated with e.m. waves of a given frequency. The surface dipoles would start oscillating with the same frequency, their amplitude depending on the adatom–adatom and adatom–substrate interactions. Let us make, now, contact with our simple dimer model. The SR quantifier, Y_0/F_0, plotted in Section 3, plays the role of an electric susceptibility. This means that the emission (absorption) power of surface dipoles can vary appreciably with the temperature substrate. However, as the electric susceptibility of the adsorbed dipoles is maximum for an optimal SR temperature, the balance of absorbed/emitted radiation is expected to drive the local substrate temperature towards the SR temperature of the dipoles. In a forthcoming publication we investigate such a feedback mechanism, where, contrary to standard SR, the temperature is no longer the control parameter. Indeed, in this picture, the stationary temperature of the surface is influenced by the dipole SR temperature and is itself controlled by the frequency and intensity of the e.m. radiation.

Acknowledgements

This work has been supported by the ESF STOCHDYN project, Spanish MICINN project FISICOS (FIS2007-60327), Govern Balear, and FEDER (E.H.), the EU NoE BioSim, LSHB-CT-2004-005137 (M.P.), the Estonian Ministry of Education and Research through project no. SF0690030s09 and the Estonian Science Foundation via Grant no. 7466 (M.P., E.H.).

References

[1] J.S. Bader et al., Proc. Natl. Acad. Sci. 96 (1999) 13165.
[2] C. Bustamante, J. Liphardt, F. Ritort, Phys. Today 58 (7) (2005) 43.
[3] M. Patriarca, P. Szelestey, E. Heinsalu, Acta Phys. Pol. B 36 (2005) 1745.
[4] E. Heinsalu, M. Patriarca, F. Marchesoni, Phys. Rev. E 77 (2008) 021129.
[5] A. Pototosky, N. Janson, F. Marchesoni, S. Savel'ev, EPL 88 (2009) 30003.
[6] P. Hänggi, F. Marchesoni, Rev. Mod. Phys. 81 (2009) 387.
[7] M. Borromeo, F. Marchesoni, Chaos 15 (2005) 026110.
[8] Q.H. Wei, C. Bechinger, P. Leiderer, Science 287 (2000) 625;
C. Lutz, M. Kollmann, C. Bechinger, Phys. Rev. Lett. 93 (2004) 026001.
[9] R. Gommers, S. Denisov, F. Renzoni, Phys. Rev. Lett. 96 (2006) 240604;
R. Gommers, S. Bergamini, F. Renzoni, ibid. 95 (2005) 073003.
[10] J.F. Wambaugh, C. Reichhardt, C.J. Olson, F. Marchesoni, F. Nori, Phys. Rev. Lett. 83 (1999) 5106.
[11] D.A. Doyle et al., Science 280 (1998) 69.
[12] B. Alberts et al., Molecular Biology of the Cell, Garland, New York, 1994.
[13] J. Kärger, D.M. Ruthven, Diffusion in Zeolites and Other Microporous Solids, Wiley, New York, 1992;
S. Matthias, F. Muller, Nature 424 (2003) 53;
Z. Siwy, A. Fulinski, Phys. Rev. Lett. 89 (2002) 198103.
[14] F. Marchesoni, Phys. Lett. A 231 (1997) 61.
[15] L. Gammaitoni, P. Jung, P. Hänggi, F. Marchesoni, Rev. Mod. Phys. 70 (1998) 223.
[16] for an update see L. Gammaitoni, P. Hänggi, P. Jung, F. Marchesoni, Special issue on stochastic resonance, Eur. Phys. J. B 69 (2009) 1.
[17] A.H. Romero, A.M. Lacasta, J.M. Sancho, Phys. Rev. E 69 (2004) 051105.
[18] T.E. Dialynas, G.P. Tsironis, Phys. Lett. A 218 (1996) 292.
[19] J.L. Mateos, Physica D 168–169 (2002) 205.
[20] O.M. Braun, Phys. Rev. E 63 (2000) 011102;
C. Fusco, A. Fasolino, Thin Solid Films 428 (2003) 34.
[21] J.L. Mateos, Physica A 351 (2005) 79.
[22] J. Menche, L. Schimansky-Geier, Phys. Lett. A 359 (2006) 90.
[23] E. Pijper, A. Fasolino, Phys. Rev. B 72 (2005) 165328.
[24] S. Martens, D. Hennig, S. Fugmann, L. Schimansky-Geier, Phys. Rev. E 78 (2008) 041121.
[25] P. Kloeden, E. Platen, Numerical Solutions of Stochastic Differential Equations, Springer, Berlin, 1999.
[26] E. Heinsalu, M. Patriarca, F. Marchesoni, Eur. Phys. J. B 69 (2009) 19.